J Mol Model (2009) 15:1371–1381
DOI 10.1007/s00894-009-0513-2

ORIGINAL PAPER

DFT investigation of the 1-octene metathesis reaction mechanism with the Phobcat precatalyst

Frans T. I. Marx · Johan H. L. Jordaan · Hermanus C. M. Vosloo

Received: 28 December 2008 / Accepted: 6 March 2009 / Published online: 31 May 2009

Abstract The productive self-metathesis reaction of 1-octene in the presence of the Phobcat precatalyst [$RuCl_2$(Phoban-Cy)$_2$(=CHPh)] using density functional theory was investigated and compared to the Grubbs 1 precatalyst [$RuCl_2$(PCy_3)$_2$(=CHPh)]. At the GGA-PW91/DNP level, the geometry optimization of all the participating species and the PES scans of the various activation and catalytic cycles in the dissociative mechanism were performed. The formation of the catalytically active heptylidene species is kinetically and thermodynamically favored, while the formation of *trans*-tetradecene is thermodynamically favored.

Keywords Alkene metathesis · DFT · Grubbs 1 · Molecular modeling · Phobcat

Abbreviations

ΔE	Energy difference
CM	Cross-metathesis
CPU	Central processing unit
Cy	Cyclohexyl group, C_6H_{11}
DFT	Density functional theory
DNP	Double numeric polarized
GGA	Generalized gradient approximation
Grubbs 1	Grubbs' first generation catalyst [(PCy_3)$_2$$Cl_2$Ru=CHPh]
Grubbs 2	Grubbs' second generation catalyst (H_2IMes)(PCy_3)Cl_2Ru=CHPh]
H_2IMes	1,3-bis-(2,4,6-trimethylphenyl)-2-imadazolidinylidene
^{1}H-NMR	Proton magnetic resonance spectroscopy
HDD	Hard disk drive
IRP	Intrinsic reaction path
LST/QST	Linear synchronous transit/quadratic synchronous transit
MEP	Minimum energy pathway
Mes	1,3-bis-(2,4,6-trimethylphenyl)
NEB	Nudged elastic band
NHC	N-heterocyclic carbene
NMR	Nuclear magnetic resonance spectroscopy
PCy_3	Tricyclohexyl phosphine
PES	Potential energy surface
Ph	Phenyl group, C_6H_5
Phoban-Cy	9-cyclohexyl-9-phosphabicyclo-[3.3.1]-nonane
Phobcat	First generation Phoban Grubbs-type precatalyst [(Phoban-Cy)$_2$$Cl_2$Ru=CHPh]
PW	Perdew and Wang
RAM	Random access memory
RCM	Ring-closing metathesis
ROMP	Ring-opening polymerization
SCF	Self-consistent field
SM	Self-metathesis
SMP	Secondary metathesis product
TS	Transition state

F. T. I. Marx · J. H. L. Jordaan · H. C. M. Vosloo (✉)
Catalysis and Synthesis Research Group, Chemical Resource Beneficiation Focus Area, North-West University, Potchefstroom 2520, South Africa
e-mail: manie.vosloo@nwu.ac.za

Introduction

In recent years alkene metathesis has extensively been used for the formation of carbon-carbon double bonds [1–5]. During the catalytic reaction, linear alkenes are transformed into homologs of shorter and longer carbon chains. The ruthenium precatalysts [(PCy_3)$_2$$Cl_2$Ru=CHPh] (**I**) [6–10] and [(H_2IMes)(PCy_3)Cl_2Ru=CHPh] (**II**) [11–19] (Fig. 1),

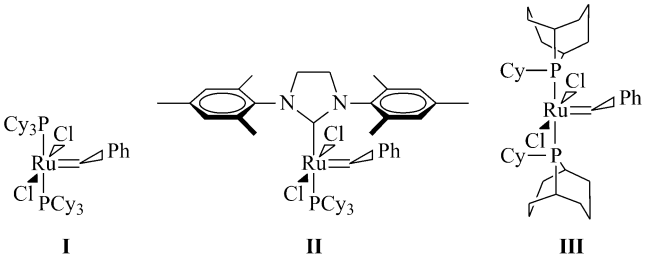

Fig. 1 Structures of Grubbs 1 (I), Grubbs 2 (II) and Phobcat (III) precatalysts

commonly referred to as the first and second generation Grubbs precatalysts, are useful for many metathesis applications such as ring-closing metathesis (RCM), cross-metathesis (CM) and ring-opening polymerization (ROMP) [20–26]. The catalytic activity and selectivity of the $[(PCy_3)_2Cl_2Ru{=}CHPh]$ (**I**) precatalyst toward primary metathesis products of the 1-octene metathesis reaction were reported to be high even at an alkene/Ru molar ratio of 10000 [27, 28]. Replacement of the phosphine ligand(s) by N-heterocyclic carbene (NHC) ligands improved the lifetime reactivity and selectivity of the metal carbene complex even further [29]. This is due to the bulkiness and increased basicity of the NHC-ligand compared to PCy_3 [12]. In contrast to their successful use in organic synthesis, the application of the first and second generation precatalysts on an industrial scale has too date not been successfully demonstrated [30]. For example, the self-metathesis (SM) of linear unfunctionalized α-olefins catalyzed by first generation Grubbs precatalysts display relatively short life times at temperatures above 50 °C [31]. Although the second generation systems display enhanced activity and thermal stability relative to first generation precatalysts, the formation of secondary metathesis products (SMPs) under certain circumstances can be a significant cause of low selectivities in these systems [16, 18, 32–38]. In an attempt to alleviate these concerns and to improve catalyst life time, the development of a new first generation Phoban Grubbs-type precatalyst, "Phobcat" $[(Phoban\text{-}Cy)_2Cl_2Ru{=}CHPh]$ (**III**), bearing Phoban-Cy (9-cyclohexyl-9-phosphabicyclo-[3.3.1]-nonane) instead of PCy_3 as ligands (Fig. 1), which exhibits significant improved stability and conversion compared to traditional first generation precatalysts was reported [30, 31, 39, 40].

The Hérisson-Chauvin metal carbene mechanism is the generally accepted mechanism for the alkene metathesis reaction (Fig. 2) [41]. The mechanism consists of successive [2+2]- cycloadditions followed by cycloreversions. This involves the coordination of the alkene to the metal center to form a π-complex followed by the formation of a metallacyclobutane intermediate, which in turn can revert to a new π-complex to yield the products after dissociation.

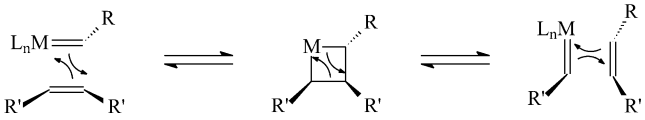

Fig. 2 A [2+2]-cycloaddition between a transition metal alkylidene and an alkene

Although many aspects of the alkene metathesis mechanism in the presence of **I** were elucidated by various techniques including kinetic measurements [9, 42, 43], there are still aspects that need to be investigated. This includes determining the species that is the most active in the metathesis reaction as well as elucidating the mechanism when the benzylidene and not the methylidene are used as precatalyst. The alkene metathesis reaction with Ru–carbene complexes has been studied by molecular modeling using simple substrates and simplified ligands. Adlhart and Chen [44] have summarized the mechanistic pathways, which can be divided into two main categories, i.e., an associative and dissociative mechanism. Recent studies indicate that the dissociative mechanism, which is initiated by the dissociation of a phosphine ligand from $RuX_2(PR_3)_2(=CHR)$ to form a 14-electron species, is preferred [43–45]. Chen and co-workers [46] confirmed this by the identification of the 14-electron species by gas-phase mass spectrometry. The rate of phosphine dissociation and initiation of the alkene metathesis reaction by $RuX_2L(PR_3)(=CHR)$ type precatalysts have been investigated theoretically and experimentally by Sanford et al. [43].

Theoretical studies performed in our laboratories showed the usefulness of molecular modeling in supporting observed ^1H NMR and other experimental results [47]. These studies were useful to gain insight into the complete productive mechanism of the 1-octene metathesis reaction with **I**. The modeling results indicated that the formation of the heptylidene species was kinetically and thermodynamically more favorable than the formation of the methylidene species.

The only theoretical studies performed on Phobcat to date consist of rotational isomerism studies and decomposition behavior of the methylidene species [30, 40]. There have been no studies on the complete mechanism of 1-octene metathesis with the first generation Phobcat precatalyst.

In this study we report on our findings regarding the mechanism of 1-octene metathesis with the first generation Phobcat precatalyst **III**. Using a DFT conceptual model the complete mechanism is presented. The results from our quantum-mechanical calculations are presented and compared to those previously reported for Grubbs 1 (**I**) [47] to gain an insight into the complete productive mechanism of the 1-octene metathesis reaction with Grubbs-type precatalysts. Our results are also compared to some of the observed experimental results reported previously for Phobcat [30, 31, 39, 40, 48].

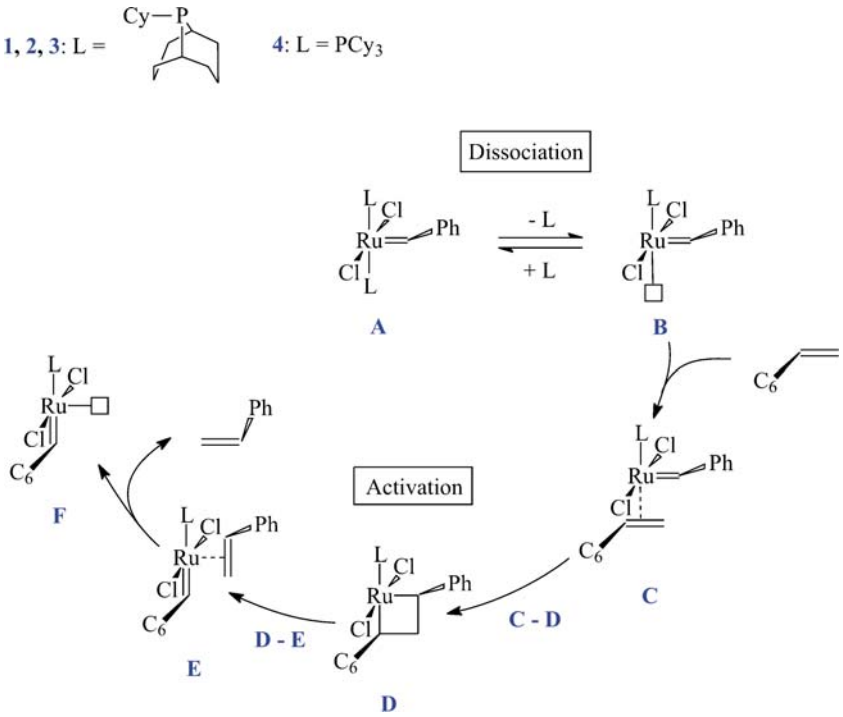

Fig. 3 The dissociation (**A** to **B**) and activation (**B** to **F**) steps in the mechanism of productive 1-octene metathesis using **A1**, **A2**, **A3** and **A4**

Computational details

Hardware

Two types of hardware were used for the molecular modeling: two personal computers with one CPU and one cluster with 52 CPU's.

The specifications of the personal computers (HP) were as follows:

Operating system: Microsoft Windows XP with Service Pack 2
Processor: Intel Pentium 4, 3.0 GHz
Memory: 1.5 GB RAM

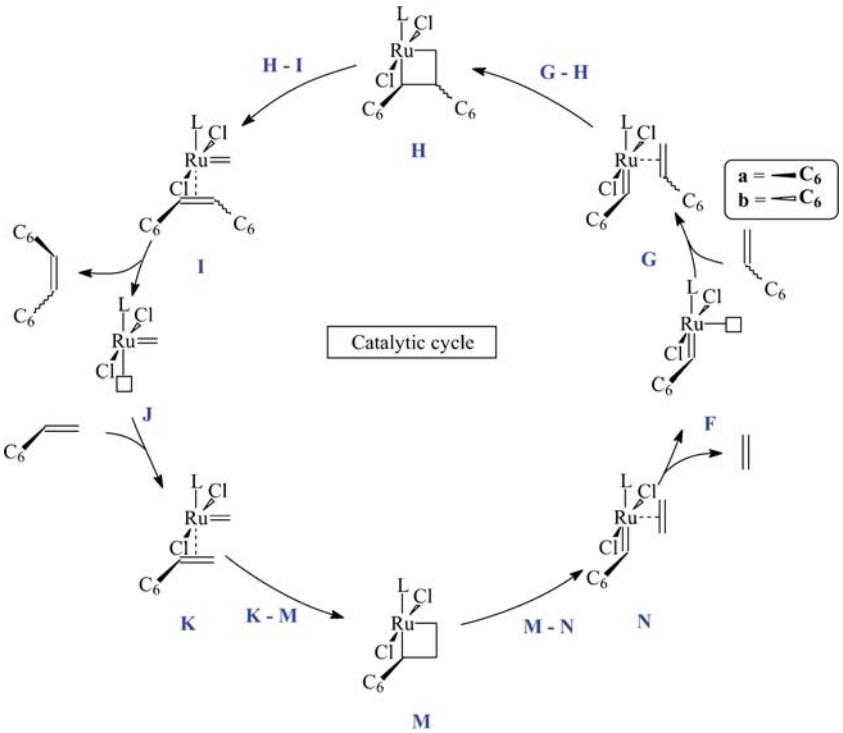

Fig. 4 Catalytic cycle in the mechanism of productive 1-octene metathesis using **A1**, **A2**, **A3** and **A4**

Table 1 Theoretical values of key bond lengths and angles of Grubbs 1 and Phobcat

	Grubbs 1	Grubbs 1		Phobcat (A1)	
	Nguyen [59]	Jordaan [47]	Calculated[a]	Dwyer [40]	Calculated[a]
Bond lengths (Å)					
Ru=C	1.838	1.878	1.877	-	1.882
Ru-Cl_{avg}	2.390	2.452	2.451	-	2.453
Ru-P_{avg}	2.416	2.490	2.491	2.445	2.445
Bond angles (°)					
Cl-Ru-Cl	168.21	160.97	160.51	-	167.65
P(1)-Ru-P(2)	161.90	163.35	163.72	159.60	159.56
Ru=C-R	136.70	136.04	136.10	-	137.03

[a] $DMol^3$ GGA/PW91/DNP – full DFT calculation of geometries

The specifications of the cluster were as follows:

52 CPU cluster (HP Proliant CP4000 Linux Beowulf with Procurve Gb/E Interconnect on compute nodes):
1× Master node: HP DL385 – 2×2.8 MHz AMD Opteron 64,
2 GB RAM, 2×72 GB HDD
12× Compute nodes: HP DL145G2 – 2×2.8 MHz AMD Opteron 64,
2 GB RAM, 2×36 GB HDD
Operating system on compute nodes: Redhat Enterprise Linux 4
Cluster operating system: HPC CMU v3.0 cluster.

Software

The quantum-chemical calculations were carried out by density functional theory (DFT) since it usually gives realistic geometries, relative energies and vibrational frequencies for transition metal compounds. All calculations were performed with the $DMol^3$ DFT code [49–51] as implemented in Accelrys Materials Studio 3.2 and 4.2. [52]. The non-local generalized gradient approximation (GGA) functional by Perdew and Wang (PW91) [53] was used for all geometry optimizations. The convergence criteria for these optimizations consisted of threshold values of 2×10^{-5} Ha, 0.004 Ha/Å and 0.005 Å for energy, gradient and displacement convergence, respectively, while a self-consistent field (SCF) density convergence threshold value of 1×10^{-5} Ha was specified. $DMol^3$ utilizes a basis set of numeric atomic functions, which are exact solutions to the Kohn-Sham equations for the atom [54]. These basis sets are generally more complete than a comparable set of linearly independent Gaussian functions and have been demonstrated to have small basis set superposition errors [54]. In this study a polarized split valence basis set, termed double numeric polarized (DNP) basis set has been used. All geometry optimizations employed highly efficient delocalized internal coordinates [55]. The use of delocalized coordinates significantly reduces the number of geometry optimization iterations needed to optimize larger molecules compared to the use of traditional Cartesian coordinates. Some of the geometries optimized were also subjected to full frequency analyses at the same GGA/PW91/DNP level of theory to verify the nature of the stationary points. Equilibrium geometries were characterized by the absence of imaginary frequencies. Preliminary transition state (TS) geometries were obtained by the integrated linear synchronous transit/quadratic synchronous transit (LST/QST) algorithm available in Materials Studio 3.2 and 4.2. This approach was used before in computational studies in homogeneous trimerisation and metathesis [30, 40, 56, 57]. These preliminary structures were then subjected to full TS optimizations using an eigenvector following algorithm. For selected transition state geometries confirmation calculations, involving intrinsic reaction path (IRP) calculations were performed in which the path connecting reagents, TS and products are mapped. The IRP technique used in Materials Studio 3.2 and 4.2 also corresponds to the intuitive minimum energy pathway (MEP) connecting two structures and is based on the nudged elastic band (NEB) algorithm of Henkelman and Jónsson [58]. The IRP calculations, performed at the same GGA/PW91/DNP level of theory, ensured the direct connection of transition states with the respective reactant and product geometries.

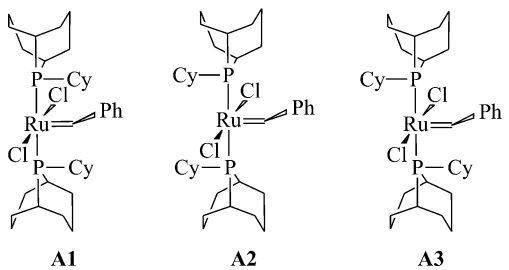

A1 **A2** **A3**

Fig. 5 Rotational isomers of Phobcat **A1**, **A2** and **A3**

All transition structure geometries exhibited only one imaginary frequency in the reaction coordinate. All results were mass balanced for the isolated system in the gas phase. The energy values that are given in the results are the electronic energies at 0 K and therefore only the electronic effects are in consideration in this paper.

Results and discussion

Model system and notations

Conceptually the productive metathesis of 1-octene in the presence of Grubbs carbene complexes is illustrated in Figs. 3 and 4. This mechanistic model is mainly based on the dissociative mechanism proposed by Grubbs et al. [43, 45], modeled by Adlhart and Chen [44] and the modeling and experimental results of Jordaan et al. [47]. The generic labels **A**-**N** are given to the individual ruthenium carbene and derived species involved in the reaction mechanism. A numerical suffix is used to differentiate between the various precatalysts, for example **A4** refers to Grubbs 1. The mechanism consists of the initial loss of a phosphine ligand from the precatalyst (**A**) to yield the 14-electron catalytic active species (**B**). This is followed by activation steps, **B**-**F** (Fig. 3), and catalytic steps, **F**-**N** (Fig. 4). The different stereochemical approaches of 1-octene toward the catalytically active species **F** leads to two catalytic cycles (**a** and **b** notations for **F** to **J** in Fig. 4). The cycle consists of several successive formal [2+2]-cycloadditions to form a metallacyclobutane and cycloreversions to form the respective catalytically active species. Before the precatalyst can enter the catalytic cycle, there is an initiation phase (activation) in which the precatalyst first has to be converted from the benzylidene complex (**A**) to the heptylidene (**F**). This takes place through the coordination of 1-octene to the metal center of the 14-electron intermediate (**B**) to form the π-complex (**C**), which undergoes a formal [2+2]-cycloaddition to form a metallacyclobutane ring (**D**) which in turn can revert to a new π-complex (**E**). The liberation of the alkene from the new π-complex leads to the new catalytically active heptylidene species (**F**) that enters the catalytic cycle. The alkyl chain points out of the plane of the page upon entering the catalytic cycle. Within the catalytic cycle the heptylidene (**F**) is converted to the methylidene (**J**), which is again converted back to the heptylidene (**F**) until all the 1-octene has been consumed or the precatalyst has decomposed. During the conversion of the heptylidene to the methylidene, *cis*- and *trans*-7-tetradecene is formed, while ethene forms when the methylidene is converted to the heptylidene.

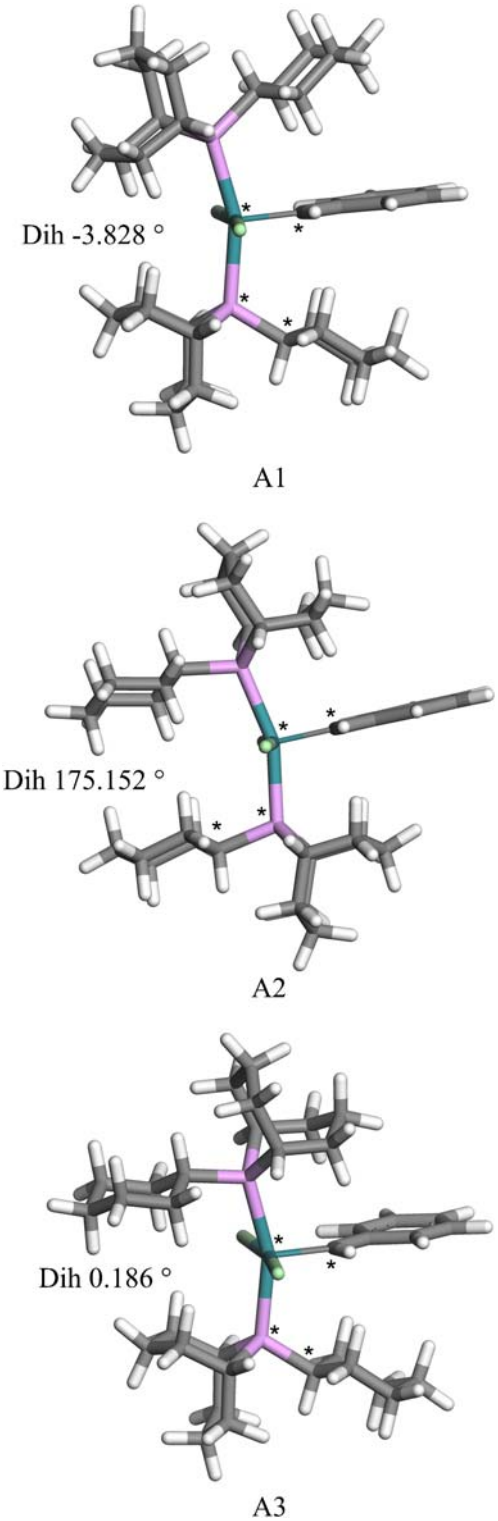

Fig. 6 The dihedral angles of **A1**, **A2**, and **A3** measured as described by Dwyer et al. [52]

Validation of computational method

To compare different Grubbs-type precatalysts it is necessary to get a better idea of the validity of the computational

Table 2 The energy difference (kcal mol^{-1}) between the rotational isomers of Phobcat

	Cisoid-cisoid (A1)	*Transoid-transoid* (A2)	*Cisoid-transoid* (A3)
Dwyer [52]	2.22	0.00	0.72
Calculated[a]	2.22	0.00	0.65

[a] $DMol^3$ GGA/PW91/DNP – full DFT calculation of geometries

method. To do this we compared calculated key bond lengths and angles of both Grubbs 1 and Phobcat with those reported by Jordaan et al. [47] and Dwyer et al. [40] (Table 1). A good correlation was obtained. Jordaan et al. [47] reported that an acceptable correlation is obtained between calculated and crystallographic data when bond lengths and angles are compared. From Table 1 it is clear that our calculated values are nearly identical to those obtained by Jordaan et al. [47] and the limited values of Dwyer et al. [40]. The small differences in calculated values can be attributed to small differences in the calculation methods. What can also be seen is that the bond lengths and bond angles of Grubbs 1 and Phobcat are in the same order. The average Ru-P bond length of Phobcat is 0.046 Å shorter than those of Grubbs 1. This would suggest a stronger Ru-P bond might be present which is consistent with observed experimental data [31]. In the underlying sections the individual phases and steps of the mechanism will be discussed under the following headings:

- Initiation step,
- Activation step,
- Catalytic cycle.

Initiation step

Initiation takes place when one of the phosphine ligands dissociates from the precatalyst (**A**) to produce the 14-electron catalytic active species (**B**). The possibility of rotational isomerism of Phobcat has already been reported by Dwyer et al. [40]. We conducted a conformer search as described by Dwyer et al. [40] and calculated nearly identical energy values for the respective conformers.

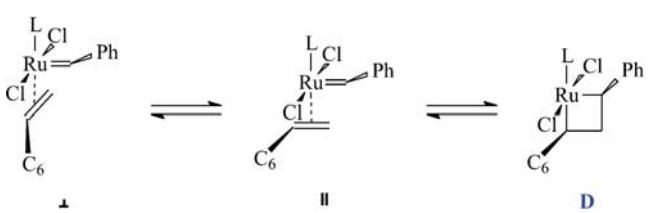

Fig. 7 Alkene coordination in the dissociative pathway

Calculations were conducted on a series of structures of which the dihedral angle of $C_{carbene}$-Ru-P_{bottom}-C_{Cy} in **A2** was incrementally changed by 20° to complete a full rotation of the lower cyclohexylphoban ligand through 360°. Only the scenario for rotation of one ligand was considered. The top cyclohexylphoban ligand was left unchanged (and unconstrained) along the *transoid* P-Cy/$C_{carbene}$ orientation. The orientation of the cyclohexyl rings on the phosphine ligands with respect to the benzylidene moiety is used to differentiate between the different rotational isomers. The orientation is illustrated in Fig. 5, both cyclohexyl rings *cisoid* (**A1**), both cyclohexyl rings *transoid* (**A2**), one cyclohexyl ring lying *cisoid* and one cyclohexyl ring lying *transoid* (**A3**).

Upon identifying the lowest energy rotational isomers we performed a geometry optimization calculation without any constrains in place on any of the ligands. The resulting dihedral angles are illustrated in Fig. 6. A comparison of our calculated values of the energy differences between the three geometry optimized isomers of Phobcat and those of Dwyer et al. [40] is given in Table 2. The small energy difference between calculated values of the *cisoid-transoid* isomers can be attributed to small differences in the calculation method and the fact that in our calculations the dihedral angle was left unconstrained. Dwyer et al. [40] concluded from their NMR experiments and calculations that **A2** would be the most abundant isomer in the crystal structure, since it is the energetically more favorable structure. This however does not account for the catalytic activity of the precatalyst. Which rotational isomer is the most active precatalyst is a question that still needs to be addressed.

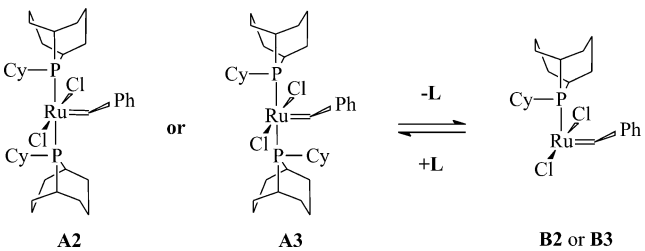

Fig. 8 Ligand dissociation from **A2** and **A3** to yield the identical product **B2** or **B3**

Table 3 Comparison of electronic energies of the π-coordination intermediate containing 1-octene

Precatalyst	Energy ratios $\Delta E_{\mathbf{B\text{-}A}}/\Delta E_{\mathbf{B\text{-}C}}$	$\Delta E_{\mathbf{B\text{-}C}}$ (**B-C**) kcal mol^{-1}
A1	2.14	−14.06
A2	1.38	−27.21
A4	2.39	−9.16

Activation step

After initiation an alkene coordinates to the unsaturated intermediate **B** to form the corresponding π-complex, **C**. According to Adlhart and Chen [44] the coordination of the alkene can be in two discrete, perpendicular orientations. In our study only the coordination parallel to the Ru=C plane was investigated, $\mathbf{C}_{\parallel}$. This correlates with a recent study by Janse van Rensburg et al. [30] which found that the parallel coordination, $\mathbf{C}_{\parallel}$, was energetically more favorable than the perpendicular coordination $\mathbf{C}_{\perp}$, (Fig. 7).

To compare the Phobcat rotational isomers with Grubbs 1 it is necessary to point out that there are essentially only two isomers worth considering. Once a ligand dissociates from the *cisoid-transoid* isomer it is identical to either the *cisoid-cisoid* or *transoid-transoid* isomer (Fig. 8). The precatalyst structure (**A**) energy difference will be a constant energy difference between the isomers. Therefore only **A1** and **A2** will be compared to Grubbs 1 (**A4**).

As Jordaan et al. [47] already pointed out the coordination of the substrate to the 14-electron species (**B-C**) is a step that is in competition with the recoordination of the phosphine ligand (**B-A**). In theoretical models there is usually only one substrate molecule competing with one phosphine, although in a catalytic system with precatalyst to substrate ratios of 1:500 or more this competition is statistically favored toward the substrate. A model usually excludes this statistical competitiveness. The competition can be described by comparing the energy of coordination of the phosphine to the energy of coordination of the substrate by taking the ratio of the respective energy differences. These values are summarized by the ratio $\Delta E_{\mathbf{B\text{-}A}}/\Delta E_{\mathbf{B\text{-}C}}$ in Table 3 for the metathesis of 1-octene with **A1**, **A2** and **A4**. From these ratios it is clear that **A2** has a very strong affinity for substrate coordination while **A1** has a weaker affinity that is almost identical to that of **A4**.

The electronic energy profiles of Phobcat and Grubbs 1 with 1-octene is compared in Fig. 9. The electronic energy of activation of **C** to **D** with 1-octene is 5.57 kcal mol^{-1} for **A1**, 16.41 kcal mol^{-1} for **A2** and 13.85 kcal mol^{-1} for **A4**. The activation of **A2** with 1-octene seems to be less favorable than **A1** and **A4**. The metallacyclobutane intermediates are in all three cases of similar thermodynamic electronic stability. The difference here is that ΔE from **C** to **D** for **A1** is −10.36 kcal mol^{-1}, for **A2** is −2.21 kcal mol^{-1} and for **A4** is −4.24 kcal mol^{-1}. This once again shows that **A2** has the smallest driving force for 1-octene activation. The other big difference between the activation routes is the dissociation of the product (styrene) to form the alkylidene species **F** (**D** to **F**). In the **A1** and **A2** route the energy increases with 23.58 kcal

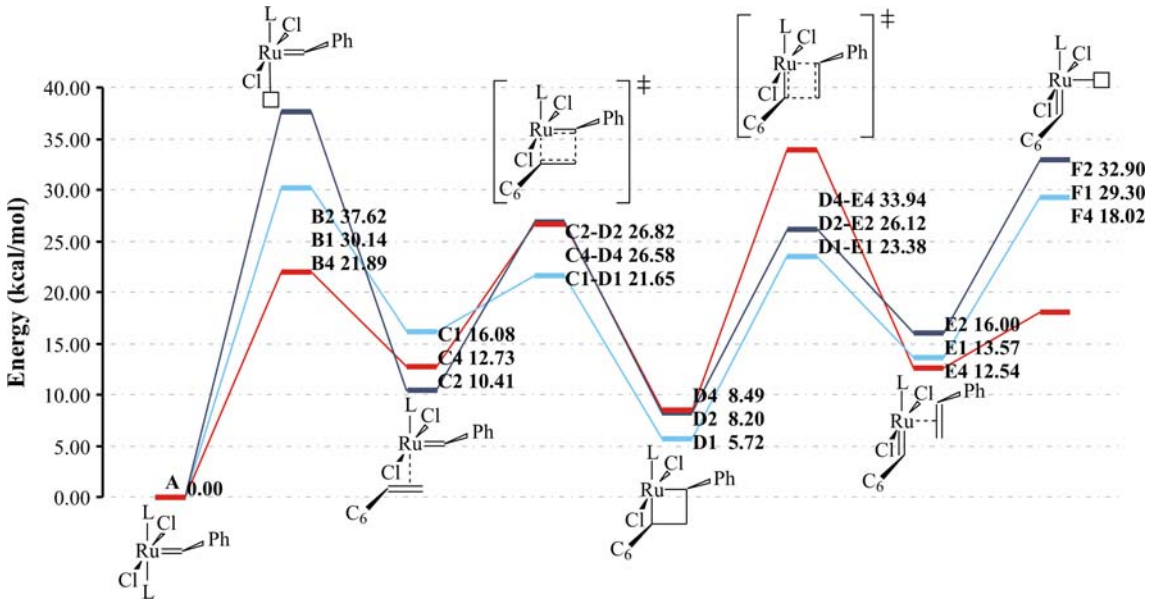

Fig. 9 Electronic energy profiles of the activation steps of the metathesis of 1-octene using Grubbs 1 and Phobcat

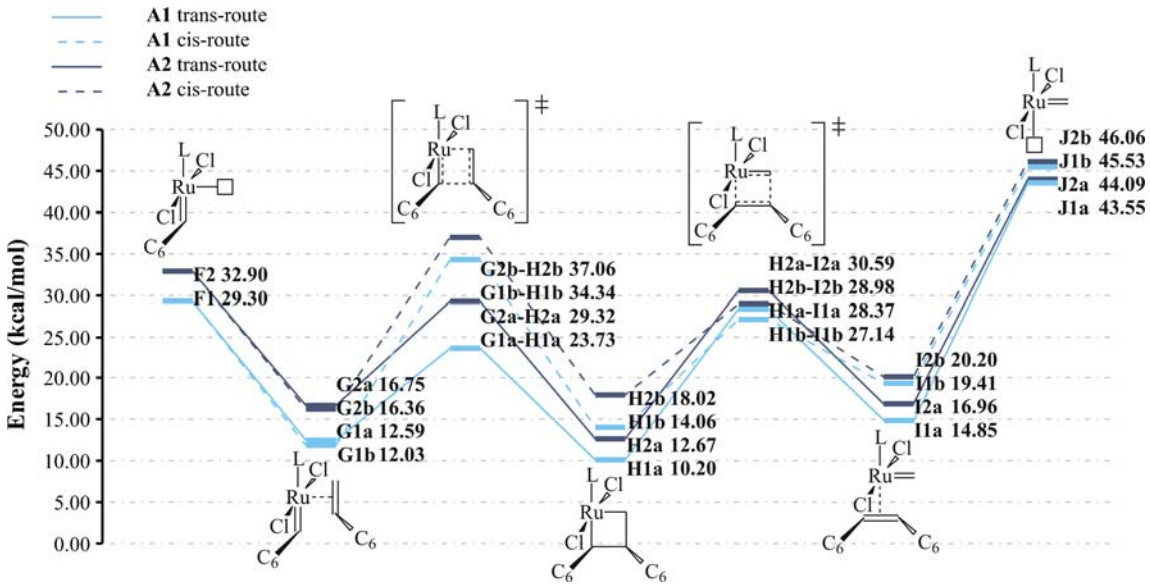

Fig. 10 Electronic energy profiles of the *cis*- and *trans*-route catalytic steps (**F** to **J**) of the metathesis of 1-octene using Phobcat

mol^{-1} (**D1**-**F1**) and 24.7 kcal mol^{-1} (**D2**-**F2**) respectively while the **A4** route requires 9.53 kcal mol^{-1} (**D4**-**F4**). This could severely hamper the activation rate of the two Phobcat isomers **A1** and **A2**. This is in agreement with the observed experimental results of Janse van Rensburg [30] which showed a slower Phobcat activation rate compared to **A4**.

Catalytic cycle

The catalytic cycle using the heptylidene **F** was investigated further; an 1-octene molecule now coordinates to the catalytically active species to yield **H**. Stereochemically this coordination can take place in two different modes, the hexyl groups *trans* and the hexyl groups *cis*. The respective energy profiles for **A1** and **A2** are illustrated in Fig. 10 (Only the *trans*-approach is illustrated). The two approaches give rise to transition states with different electronic energies, which is summarized in Table 4. The formation of the metallacyclobutane (**H**) is easier for the *trans*-routes than for the *cis*-routes. The metallacyclobutane intermediates that form then liberates the PMP's *trans*-7-tetradecene and *cis*-7-tetradecene. It would seem from this that the *trans*-route is energetically more favorable than the *cis*-route.

Table 4 The energy difference between the rotational isomers of Phobcat and Grubbs 1

Precatalyst	$\Delta E_{(\mathbf{G\text{-}H})\text{-}\mathbf{G}}$ [(**G-H**)-**G**] kcal mol^{-1}	$\Delta E_{(\mathbf{H\text{-}I})\text{-}\mathbf{H}}$ [(**H-I**)-**H**] kcal mol^{-1}
A1 ***trans*-route**	11.14	18.17
A1 ***cis*-route**	22.31	13.08
A2 ***trans*-route**	12.57	17.92
A2 ***cis*-route**	20.70	10.96
A4 ***trans*-route**	11.28	23.38

The complete catalytic cycle energy profiles of the *trans*-routes of **A1** and **A2** was compared to that of **A4** (Fig. 11). If the energy of **A1** and **A2** is compared to that of **A4** for the *trans*-route (Table 4) it is clear that both follow the same trend as **A4**. The metallacyclobutane ring (**H**) of **A1** and **A2** seems to dissociate easier than **A4**. The main difference between the two precatalysts is intermediate **J** where the catalysts have a free coordination site. The methylidenes **J1** and **J2** have energies of 43.55 kcal mol^{-1} and 44.09 kcal mol^{-1} respectively while **J4** has an energy value of only 24.08 kcal/mol. The low energy barrier of **A4** for the formation of **J** from **I** (1.84 kcal mol^{-1}) suggests that the methylidene with an open coordination site would be stable in solution for a longer time than the **A1** and **A2** methylidene. This might be a contributing factor to the thermodynamically unfavorable conversion of the **A4** methylidene [47]. The high energy barrier observed during the formation of **J**, 28.70 kcal mol^{-1} for **A1** and 27.13 kcal mol^{-1} for **A2** suggests that the formation of the Phobcat methylidene is unfavorable. The catalytic cycle would be slowed down every time this step is reached. This high barrier also suggests that the coordination of an alkene by

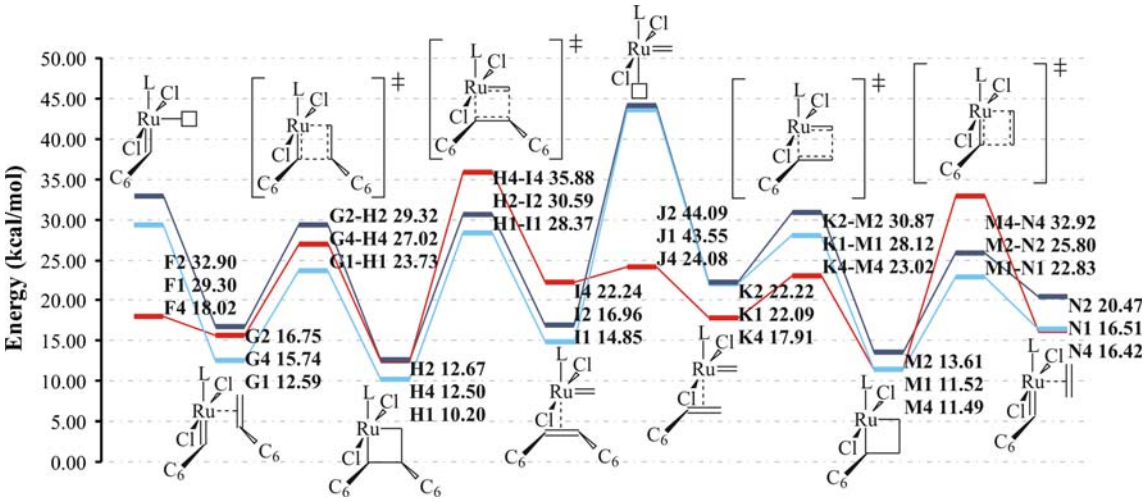

Fig. 11 Electronic energy profiles of the complete *trans*-route catalytic steps of the metathesis of 1-octene using Grubbs 1 and Phobcat

Phobcat is favored over a free coordination site. This might also be a contributing factor to the prolonged lifetime of the precatalysts [39] since it would be better protected from deactivating groups. This barrier might also explain the better stability of Phobcat at higher temperatures during reactions with alkenes [39, 48]. More energy would be needed to get over this barrier for the catalytic cycle to continue.

Finally the second half of the catalytic cycle, **J** to **N**, was modeled. The formation of the metallacyclobutane (**M**) is once again favored over the dissociation thereof (Table 5). The Phobcat catalysts are once again able to dissociate easier than Grubbs 1. This suggests that the Phobcat methylidene is catalytically more active than Grubbs 1. This supports the observed experimental results of Boeda et al. [48] and Forman et al. [39] which clearly show that Phobcat has a higher conversion ratio of 1-octene when compared to Grubbs 1. What also becomes apparent from Fig. 11 is that there appears to be little difference in catalytic activity between **A1** and **A2**. Whether this is a property of the Phoban ligand or is true for all ligands of this type can only be confirmed with further investigation. To gain deeper insight into the complete mechanism it is necessary to calculate the Gibbs free energy surfaces, since Janse van Rensburg et al. [30] determined that this gives a more accurate depiction of the mechanism.

Table 5 The energy difference (kcal mol^{-1}) between the rotational isomers of Phobcat

Precatalyst	$\Delta E_{(\mathbf{K\text{-}M})\text{-}\mathbf{K}}$ [(**K-M**)-**K**] kcal mol^{-1}	$\Delta E_{(\mathbf{M\text{-}N})\text{-}\mathbf{M}}$ [(**M-N**)-**M**] kcal mol^{-1}
A1 ***trans*-route**	6.03	11.31
A2 ***trans*-route**	8.65	12.19
A4 ***trans*-route**	5.11	21.43

Conclusions

Using DMol^3 density functional theory calculations we have described the 1-octene metathesis reaction catalyzed by the Phobcat precatalyst *via* a dissociative mechanism. The DMol^3 density functional theory calculations compared well with calculations by other authors. We also found that the same simple models that effectively describe the metathesis of simple substrates with methylidene type catalysts cannot be used to describe the reaction of real systems. It is clear that the mechanism of metathesis with actual catalytic systems are complex if it is done with large substrates like 1-octene and that electronic effects cannot fully account for effects that are observed, like the *cis*/*trans* isomerization of the primary metathesis product. Since this was a preliminary computational study of the complete catalytic cycle we could not make any clear conclusions regarding activity. What can be concluded is that the complete catalytic cycle with 1-octene is a very complex reaction and cannot just be considered by using a simple model. Further studies *via* Gibbs free energy surfaces of the complete system are necessary to fully understand this mechanism.

Acknowledgments We thank the North-West University (Potchefstroom Campus) for their financial support of our Laboratory for Applied Molecular Modeling and the National Research Foundation of South Africa for their financial contribution toward the studies of FTIM. We also thank M. Jordaan for providing us with the corrected values of her Grubbs 1 DFT calculations.

References

1. Ivin KJ, Mol JC (1997) Olefin metathesis and metathesis polymerization. Academic Press, San Diego
2. Dörwald FZ (1999) Metal carbenes in organic synthesis. Wiley-VCH, Weinheim, Germany
3. Rouhi AM (2002) Olefin metathesis: big-deal reaction. Chem Eng 80(51):29–33
4. Wagner PH (1992) Olefin metathesis - applications for the nineties. In: Chemistry and industry. Society of Chemical Industry. Available via BNET.com. http://findarticles.com/p/articles/mi_hb5255/is_n9/ai_n28615079/print?tag=artBody;col1. Accessed 14 Dec 2008
5. Fürstner A (2000) Olefin metathesis and beyond. Angew Chem Int Ed 39:3012–3043
6. Nguyen ST, Grubbs RH, Ziller JW (1993) Syntheses and activities of new single-component, ruthenium-based olefin metathesis catalysts. J Am Chem Soc 115:9858–9859
7. Schwab P, France MB, Ziller JW et al. (1995) A series of well-defined metathesis catalysts-synthesis of [RuCl2(=CHR')(PR3) 2] and its reactions. Angew Chem Int Ed 34:2039–2041
8. Schwab P, Grubbs RH, Ziller JW (1996) Synthesis and applications of RuCl2(=CHR′)$(PR_3)_2$: the influence of the alkylidene moiety on metathesis activity. J Am Chem Soc 118:100–110
9. Dias EL, Nguyen ST, Grubbs RH (1997) Well-defined ruthenium olefin metathesis catalysts: mechanism and activity. J Am Chem Soc 119:3887–3897
10. Blackwell HE, O'Leary DJ, Chatterjee AK et al. (2000) New approaches to olefin cross-metathesis. J Am Chem Soc 122:58–71
11. Weskamp T, Schattenmann WC, Speigler M et al. (1998) A novel class of ruthenium catalysts for olefin metathesis. Angew Chem Int Ed 37:2490–2493
12. Weskamp T, Kohl FJ, Hieringer W et al. (1999) Highly active ruthenium catalysts for olefin metathesis: the synergy of N-heterocyclic carbenes and coordinatively labile ligands. Angew Chem Int Ed 38:2416–2419
13. Ackermann L, Fürstner A, Weskamp T et al. (1999) Ruthenium carbene complexes with imidazolin-2-ylidene ligands allow the formation of tetrasubstituted cycloalkenes by RCM. Tetrahedron Lett 40:4787–4790
14. Weskamp T, Kohl FJ, Herrmann WA (1999) N-heterocyclic carbenes: novel ruthenium–alkylidene complexes. J Organomet Chem 582:362–365
15. Frenzel U, Weskamp T, Kohl FJ et al. (1999) *N*-Heterocyclic carbenes: application of ruthenium–alkylidenecomplexes in ring-opening metathesis polymerization. J Organomet Chem 586:263–265
16. Scholl M, Trnka TM, Morgan JP et al. (1999) Increased ring closing metathesis activity of ruthenium-based olefin metathesis catalysts coordinated with imidazolin-2-ylidene ligands. Tetrahedron Lett 40:2247–2250
17. Scholl M, Ding S, Lee CW et al. (1999) Synthesis and activity of a new generation of ruthenium-based olefin metathesis catalysts coordinated with 1, 3-dimesityl-4, 5-dihydroimidazol-2-ylidene ligands. Org Lett 1:953–956
18. Huang J, Stevens ED, Nolan SP et al. (1999) Olefin metathesis-active ruthenium complexes bearing a nucleophilic carbene ligand. J Am Chem Soc 121:2674–2678
19. Jafarpour L, Huang J, Stevens ED et al. (1999) (*p*-cymene) RuLCl2 (L) 1, 3-Bis(2, 4, 6-trimethylphenyl) imidazol-2-ylidene and 1, 3-Bis(2, 6-diisopropylphenyl) imidazol-2-ylidene) and related complexes as ring closing metathesis catalysts. Organometallics 18:3760–3763
20. Rosillo M, Dominguez G, Casarrubios L et al. (2004) Tandem enyne metathesis-Diels−Alder reaction for construction of natural product frameworks. J Org Chem 69:2084–2093
21. MatsuyaY KT, Nemoto H (2003) New strategy for the total synthesis of macrosphelides A and B based on ring-closing metathesis. Org Lett 5:2939–2941
22. Hanessian S, Margarita R, Hall A et al. (2002) Total synthesis and structural confirmation of the marine natural product dysinosin A: a novel inhibitor of thrombin and factor VIIa. J Am Chem Soc 124:13342–13343
23. Mori M, Tonogaki K, Nishiguchi NJ (2002) Syntheses of anolignans A and B using ruthenium-catalyzed cross-enyne metathesis. J Org Chem 67:224–226
24. Edwards SD, Lewis T, Taylor RJK (1999) Eight membered ethers via diene metathesis: synthetic approach to laureatin natural products. Tetrahedron Lett 40:4267–4270
25. Nicolaou KC, King NP, He Y (1998) Alkene metathesis in organic synthesis. In: Fürstner A (ed) Topics in organometallic chemistry, vol 1. Springer, New York, pp 73–104
26. Schuster M, Blechert S (1998) Transition metals for organic synthesis 1. Wiley-VHC, Weinheim, Germany
27. Van Schalkwyk C, Vosloo HCM, Du Plessis JAK (2002) A comparison of the activity of homogeneous tungsten and ruthenium catalysts for the metathesis of 1-octene. Adv Synth Catal 344:781–788
28. Dinger MB, Mol JC (2002) High turnover numbers with ruthenium-based metathesis catalysts. Adv Synth Catal 344:671–677
29. Huang J, Schanz H-J, Stevens ED et al. (1999) Influence of sterically demanding carbene ligation on catalytic behavior and thermal stability of ruthenium olefin metathesis catalysts. Organometallics 18:5375–5380
30. Janse van Rensburg W, Steynberg PJ, Kirk MM et al. (2006) Mechanistic comparison of ruthenium olefin metathesis catalysts: DFT insight into relative reactivity and decomposition behavior. J Organometalic Chem 691:5312–5325
31. Forman GS, McConnell AE, Hanton MJ et al. (2004) A stable ruthenium catalyst for productive olefin metathesis. Organometallics 23:4824–4827
32. Fürstner A, Thiel OR, Ackermann L et al. (2000) Ruthenium carbene complexes with N, N'-bis(mesityl) imidazol-2-ylidene ligands: RCM catalysts of extended scope. J Org Chem 65:2204–2207
33. Wagner J, Martin Cabrejas LM, Grosssmith CE et al. (2000) Synthesis of macrolide analogues of sanglifehrin by RCM: unique reactivity of a ruthenium carbene complex bearing an imidazol-2-ylidene ligand. J Org Chem 65:9255–9260
34. Kinderman SS, Van Maarseveen JH, Schoemaker HE et al. (2001) Enamide-olefin ring-closing metathesis. Org Lett 3:2045–2048
35. Lehman SE Jr, Schwendeman JE, O'Donnell PM et al. (2003) Olefin isomerization promoted by olefin metathesis catalysts. Inorg Chim Acta 345:190–198
36. Arisawa M, Terada Y, Takahashi K et al. (2006) Development of isomerization and cycloisomerization with use of a ruthenium hydride with *N*-heterocyclic carbene and its application to the synthesis of heterocycles. J Org Chem 71:4255–4261

37. Bourgeois D, Pancrazi A, Nolan SP et al. (2002) The $Cl_2(PCy_3)$ (IMes) Ru(=CHPh) catalyst: olefin metathesis versus olefin isomerization. Organomet Chem 643–644:247–252
38. Dharmasena UL, Foucalt HM, Dos Santos EN et al. (2005) N-heterocyclic carbenes as activating ligands for hydrogenation and isomerization of unactivated olefins. Organometallics 24:1056–1058
39. Forman GS, McConnell AE, Tooze RP et al. (2005) A convenient system for improving the efficiency of first-generation ruthenium olefin metathesis catalysts. Organometallics 24:4528–4542
40. Dwyer CL, Kirk MM, Meyer WH et al. (2006) Rotational isomerism of a phoban-derived first-generation Grubbs catalyst. Organometallics 25:3806–3812
41. Herrisson JL, Chauvin Y (1971) Catalysis of olefin transformations by tungsten complexes. II. Telomerization of cyclic olefins in the presence of acyclic olefins. Makromol Chem 141:161
42. Ulman M, Grubbs RH (1998) Relative reaction rates of olefin substrates with ruthenium(II) carbene metathesis initiators. Organometallics 17:2484–2489
43. Sanford MS, Love JA, Grubbs RH (2001) Mechanism and activity of ruthenium olefin metathesis catalysts. J Am Chem Soc 123:6543–6554
44. Adlhart C, Chen P (2004) Mechanism and activity of ruthenium olefin metathesis catalysts: the role of ligands and substrates from a theoretical perspective. J Am Chem Soc 126:3496–3510
45. Sanford MS, Ulman M, Grubbs RH (2001) New insights into the mechanism of ruthenium-catalyzed olefin metathesis reactions. J Am Chem Soc 123:749–750
46. Adlhart C, Hinderling C, Baumann H et al. (2000) Mechanistic studies of olefin metathesis by ruthenium carbene complexes using electrospray ionization tandem mass spectrometry. J Am Chem Soc 122:8204–8214
47. Jordaan M, Van Helden P, Van Sittert CGCE et al. (2006) Experimental and DFT investigation of the 1-octene metathesis reaction mechanism with the Grubbs 1 precatalyst. J Mol Cat A: Chem 254:145–154
48. Boeda F, Clavier H, Jordaan M et al. (2008) Phosphabicyclononane-containing Ru complexes: efficient pre-catalysts for olefin metathesis reactions. J Org Chem 73:259–263
49. Delley B (1990) An all-electron numerical method for solving the local density functional for polyatomic molecules. J Chem Phys 92:508–517
50. Delley B (2000) From molecules to solids with the $DMol^3$ approach. J Chem Phys 113:7756–7764
51. Delley B (1996) Fast calculation of electrostatics in crystals and large molecules. J Phys Chem 100:6107–6110
52. http://www.accelrys.com/
53. Perdew JP, Wang Y (1992) Accurate and simple analytic representation of the electron-gas correlation energy. Phys Rev B 45:13244–13249
54. Delley B (1995) Modern density functional theory: a tool for chemistry. In: Seminario JM, Politzer P (eds) Theoretical and computational chemistry, vol 2. Elsevier, Amsterdam, pp 221–254
55. Andzelm J, King-Smith RD, Fitzgerald G (2001) Geometry optimization of solids using delocalized internal coordinates. Chem Phys Lett 335:321–326
56. Janse van Rensburg W, Grové C, Steynberg JP et al. (2004) A DFT study toward the mechanism of chromium-catalyzed ethylene trimerization. Organometallics 23:1207–1222
57. Janse van Rensburg W, Steynberg PJ, Meyer WH et al. (2004) DFT prediction and experimental observation of substrate-induced catalyst decomposition in ruthenium-catalyzed olefin metathesis. J Am Chem Soc 126:14332–14333
58. Henkelman G, Jónsson H (2000) Improved tangent estimate in the nudged elastic band method for finding minimum energy paths and saddle points. J Chem Phys 113:9978–9985
59. Nguyen ST, Trnka TM (2003) In: Grubbs RH (ed) Handbook of metathesis, vol 1. Wiley-VHC, Weinheim, Germany, p 61